ACS APPLIED MATERIALS & INTERFACES

Research Article

www.acsami.org

Printed Sub-100 nm Polymer-Derived Ceramic Structures

Binh Duong,[†] Palash Gangopadhyay,[‡] Josh Brent,[‡] Supapan Seraphin,[§] Raouf O. Loutfy,[#] Nasser Peyghambarian,[‡] and Jayan Thomas*[,†,∥]

[†]NanoScience Technology Center, University of Central Florida, Orlando, Florida 32826, United States

[‡]College of Optical Sciences, The University of Arizona, Tucson, Arizona 85721, United States

[§]Department of Materials Science & Engineering, The University of Arizona, Tucson, Arizona 85721, United States

[#]Materials and Electrochemical Research Corporation, 7960 S. Kolb Road, Tucson, Arizona 85706, United States

[∥]CREOL, College of Optics and Photonics and Department of Material Science and Engineering, University of Central Florida, Orlando, Florida 32826, United States

ABSTRACT: We proposed an unconventional fabrication technique called spin-on nanoprinting (SNAP) to generate and transfer sub-100 nm preceramic polymer patterns onto flexible and rigid substrates. The dimensions of printed nanostructures are almost the same as those of the mold, since the ceramic precursor used is a liquid. The printed patterns can be used as a replica for printing second-generation structures using other polymeric materials or they can be further converted to desirable ceramic structures, which are very attractive for high-temperature and harsh environment applications. SNAP is an inexpensive parallel process and requires no special equipment for operation.

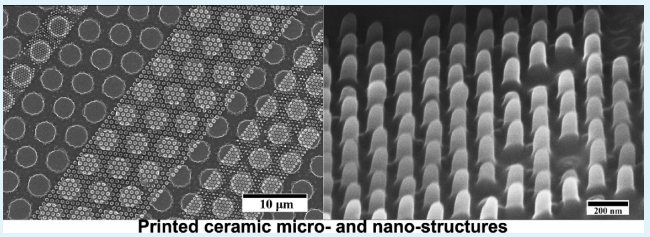

Printed ceramic micro- and nano-structures

KEYWORDS: *nanostructured ceramics, nanoimprinting, sub-100 nm ceramic structures, polymer-derived ceramics, SNAP technique, polyureasilazane*

1. INTRODUCTION

Production of novel multifunctional inorganic materials with a tailor-made, nanoscale structure is of considerable interest in semiconductor,[1−4] electronic,[5] and photonic applications.[6−8] Modern technologies have created a need for the development of new materials and patterning technologies that can provide sub-100 nm resolution, high pattern fidelity, improved reproducibility, and high throughput at low costs.[9,10] Furthermore, the increasing miniaturization of components calls for new process technologies that allow the reliable, large-scale production of materials at nanometer scale in a very cost-efficient manner. In order to achieve this ambitious goal, inorganic−organic hybrid materials, as well as amorphous and polycrystalline ceramics, which are the materials of choice for many of these applications, should be mass-produced using techniques as simple as nanoimprinting. Possible applications for nanoceramic materials are key technologies of the 21st century including electronics, photonics, and information technology, as well as microelectromechanical or nano-electromechanical systems.[11−14]

Advanced ceramics are very attractive for electronic applications, because they can operate at high power, at high temperatures, and in harsh environments. They exhibit combinations of properties, such as electrical insulation and magnetism, that are not possible in other materials.[15−18] Although scientifically interesting, possible fields of practical applications are enabled only if the ability to fabricate ceramics into nanoscale structures can be achieved via some simple techniques. Conventionally, ceramic structures are mechanically shaped using methods such as surface micromachining, pressing, or powder injection molding. However, the smallest reported feature created by these techniques was 0.1 mm in size.[19] In addition, they are time-consuming and expensive to manufacture, and they require intensive effort to produce precise microparts. These drawbacks were resolved with the successful transformation of polymers such as polysilazane, polysiloxanes, and polycarbosilanes into ceramics by thermal pyrolysis, known as polymer-derived ceramics (PDCs).[20] The preceramic polymers offer the ease of fabrication and high tailorability of chemical composition on a molecular level.[21,22] It should be noted that the polymer precursor can easily be converted to SiO_2, SiC, or Si_3N_4 by changing pyrolysis environments at a higher temperature.[23] For example, heating in the presence of ammonia and nitrogen can convert polysilazane to Si_3N_4[23] while exposing the precursor to steam can produce SiO_2.[24]

The two main routes to fabricate ceramic structures from polymer precursor are (i) photolithographic techniques[25] and (ii) nonphotolithographic methods (such as microtransfer molding (μTM),[26] micromolding in capillaries (MIMIC), and nanoimprint lithography (NIL)[27]). In standard photolithography, desired patterns are created by exposing a ceramic

Received: February 14, 2013
Accepted: April 9, 2013
Published: April 9, 2013

precursor to an energetic radiation source such as ultraviolet (UV), ion-beam, or electron-beam radiation. It has been reported that, using UV lithography, the smallest defect-free Si_3N_4 structures (with a diameter of <50 μm and a thickness of 20 μm) could be obtained after pyrolysis.[28] Although a technique such as electron-beam (e-beam) lithography is capable of making features at the sub-20 nm level, this direct structuring approach is not economically viable for high-volume production, because of the high capital and operating costs that are involved.

The conceptual novelty and technical capabilities of nonlithographical methods have been greatly adopted in fabricating various microscaled and nanoscaled devices. In the nonphotolithography category, NIL clearly stands out as the most promising technique that can provide sub-100 nm resolution, high fidelity, and high-throughput at a low cost.[29] However, there are critical processing factors limiting the use of this approach in the fabrication of PDC nanostructures.[30] In thermal-NIL (T-NIL), the mold is usually made of silicon with desired structures fabricated by e-beam lithography. A high-molecular-weight (high-M_w), solid thermoplastic polymer film that has been cast on a substrate is heated above the glass-transition temperature (T_g) to reach a viscous flow state[31] and the hard mold is pressed into the substrate under high pressure (~50−100 bar). This is followed by cooling the patterned polymer below its T_g before the mold is released. Although low-M_w polymers can be used in T-NIL, printed structures are often brittle, possibly causing fractured structures during the demolding step. T-NIL of preceramic polymers presents additional challenges, because they are thermosetting materials. A prior study reported that it was impossible to obtain direct replication of PDC microstructures from a silicon master mold, because of cracking and fragmentation during cross-linking.[32] UV-NIL is an alternative method to print structures that prevent the use of the high temperatures and pressures required in T-NIL by using liquid precursors, which can be cross-linked at room temperature under UV light. However, this process requires the mold or substrate to be transparent to UV light. To the best of our knowledge, UV-NIL was used to produce only ceramic precursor nanostructures,[33] but was never successfully converted to ceramics. Here, we demonstrate the spin-on nanoprinting (SNAP) technique, which is an easy but prudent technique to print nanostructures from preceramic polymer and convert them to ceramics. It is a benchtop procedure that can be undertaken by any unskilled personnel in the art.

2. EXPERIMENTAL SECTION

Materials and Fabrication of PDC Structures. Because of the high thermosetting temperature of polyureasilazane (PUS, commercially known as Ceraset, Kion Corp.), ~400 °C, a thermal initiator—dicumyl peroxide—was added to lower the curing temperature to 150−200 °C. The chemical structure of the precursor is shown in Figure 1. The mixture was then filtered (using a 0.2-μm filter) and degassed for an hour before use, to prevent bubble formation during thermal cross-linking. Figure 2 illustrates the printing process. The silicon master mold was first wetted with a commercially available antiadhesive agent (Rain-X). Rain-X is isopropanol-based cocktail of quaternary ammonium and fatty acid siloxanes[34] and imparts a good degree of hydrophobicity on SiO on silicon or SiO_2 surfaces.[35] This hydrophobic coating is antiadhesive in nature and helps lower the surface energy to efficiently spread and fill the nanostructured features.[36] Then, the precursor solution was dropcast onto the mold, which was preheated on a hot plate at 190 °C. The substrate was placed on top of the mold after PUS was cured for ~30 s. A longer

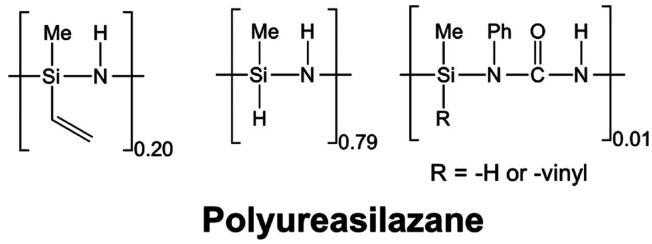

Figure 1. Chemical structure of polyureasilazane (PUS).[23]

curing time would result in a thicker film. A small pressure was applied to remove excess material between the two substrates. The compact structure was allowed to cool before the mold was separated from the substrate with the nanostructures. In this study, we used four different substrates: glass, silicon, tungsten foil, and carbon cloth. Thick freestanding preceramic films (millimeter scale) were also prepared by carefully removing the films right after the precursor solidified. To obtain thin freestanding films, we used a sacrificial layer (polyvinyl alcohol, PVA) or gelatin[37] coated on top of the substrates (silicon/glass), followed by steps 1 and 2 shown in Figure 2. Substrates with a sacrificial layer and printed PUS were then immersed in boiled water to dissolve the sacrificial layers. These aforementioned steps were carried out in air. To convert the cross-linked samples to ceramics, typical PDC pyrolysis was carried out. The samples (films on silicon substrates, carbon cloth, and freestanding films) were pyrolyzed in an argon atmosphere with a heating rate of 1 °C/min from room temperature to 600 °C, then 3 °C/min to 1100 °C with a holding time of 2 h at each stage.

Characterization of Printed Ceramic Structures. Scanning electron microscopy (SEM, H-4800) was used to characterize the morphology of the microstructures and nanostructures. An SEM microscope system coupled with energy-dispersive X-ray spectroscopy (EDS) was utilized to determine the elemental composition of the sample. Fourier transform infrared (FTIR) and Raman spectroscopy were employed to characterize structural changes. To collect infrared (IR) spectra, a thin layer of the liquid PUS was obtained by placing a drop of the liquid PUS between the two KBr plates. For the solid samples (cross-linked PUS and pyrolyzed PUS), they were ground into fine powders. The mixture of ~1% powder and KBr powder (Sigma−Aldrich, FTIR grade) was ground again. A small amount of the mixture was placed in a die and pressed to form a pellet. KBr pellets were prepared for IR spectra collection. Raman spectroscopy (Structural and Chemical Analyzer (SCA), SEM-SCA, Renishaw, U.K.) has a wavelength of 514 nm, energy of 2.41 eV, power of 50 mW, and a beam diameter of ~1 μm. Crystallization behavior of the cross-linked and pyrolyzed samples was monitored by X-ray diffraction using monochromatic Cu Kα (Scintag XDS 2000 PTS Diffractometer).

3. RESULTS AND DISCUSSION

To demonstrate the capability of our SMAP technique, preceramic nanostructures with different aspect ratios were fabricated as shown in Figure 3. We have successfully transferred the defect-free precursor films onto both rigid substrates (glass and silicon) and flexible substrates (tungsten foil and carbon cloth), as well as freestanding preceramic films. All the printed preceramic structures were stable on the substrates, even after a year. It is worth pointing out that the master mold was not damaged, even after more than 20 repetitive printings. Moreover, this technique can be used to fabricate both amorphous and crystalline silicon-based ceramic device structures. In order to demonstrate that it can be used to print any versatile structure, we have printed a photonic crystal-type structure and converted it to a ceramic, as shown in Figure 4. According to the supplier, the mass conversion of polymer to ceramic, as measured by thermogravimetric analysis (TGA), is

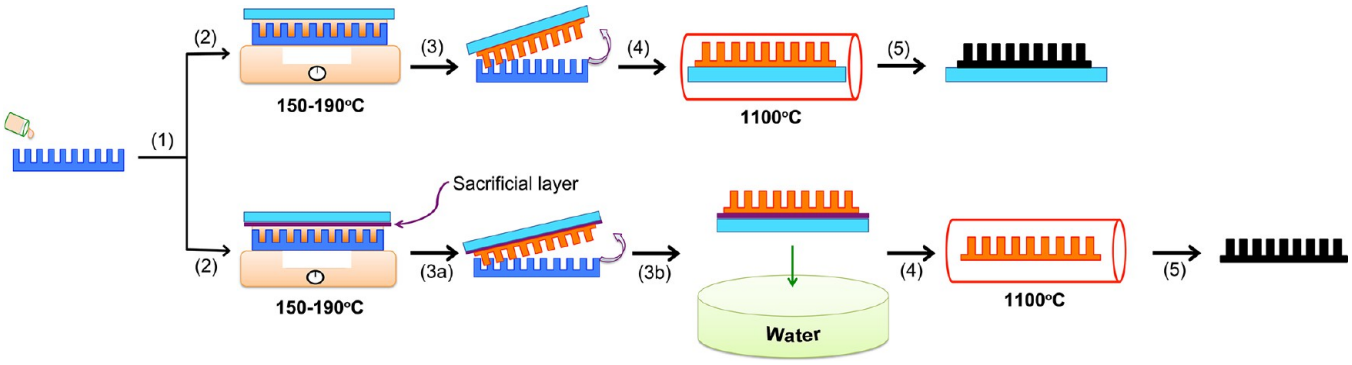

Figure 2. Schematic illustrating the steps involved in the PDC printing process. (1) First, the silicon mold is wetted with a commercially available antiadhesive agent. The solution of polyureasilazane (PUS) mixed with 1 wt % dicumyl peroxide is cast onto the preheated mold. The preceramic polymer is partially cured for ~1 min before a substrate is placed on top of the mold. (2) The compact structure is further cured at 190 °C before cooling it to room temperature. Steps 1 and 2 are carried out in air. (3) The transferred substrate is carefully separated from the mold. (4) The printed sample is converted to an amorphous ceramic by heating it to 1100 °C in an argon atmosphere. (5) $SiO_xC_yN_z$ is obtained. Similar procedure is followed to prepare freestanding ceramic films. However, the substrate is first coated with a sacrificial layer before use. After step 3a, this layer is removed by soaking the sample into hot water.

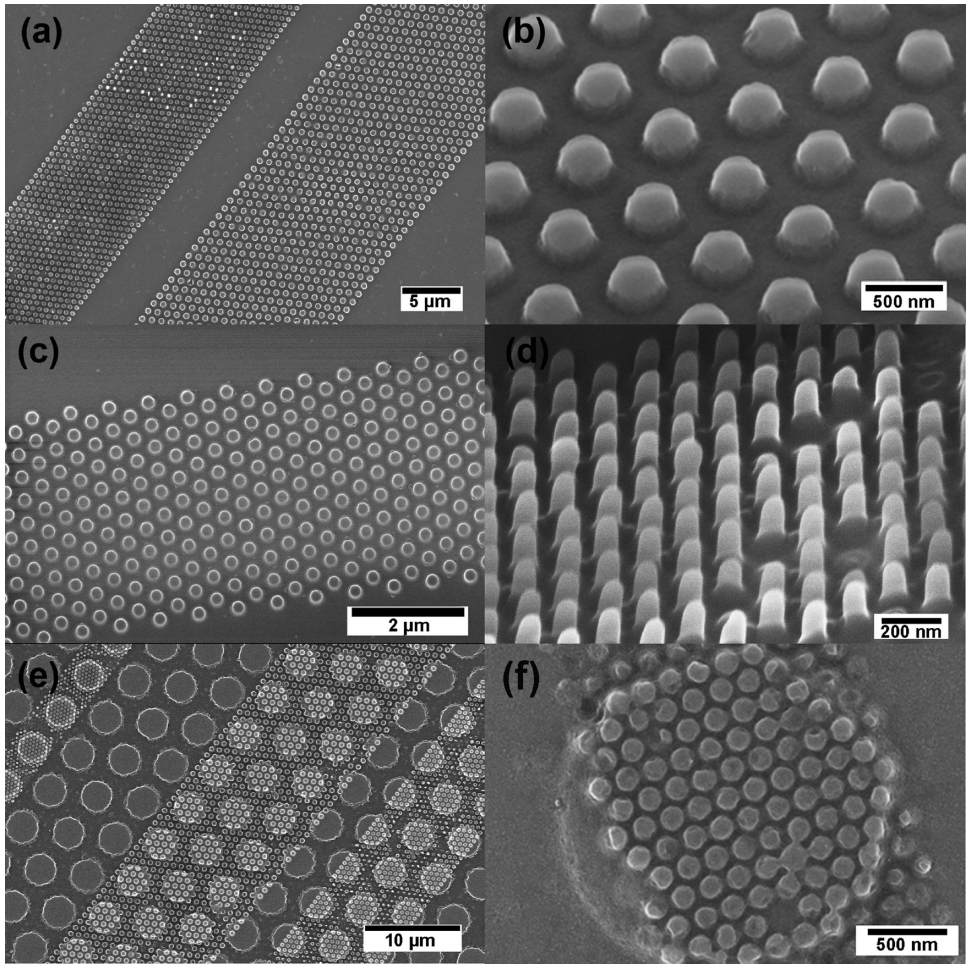

Figure 3. (a) Arrays of nanopillars with diameters of 300 and 500 nm. (b) Higher-magnification view of the 300-nm features. (c) Micrograph showing the top view of the 80-nm-diameter nanopillars. (d) Micrograph showing the 45°-angle view of the 80-nm-diameter nanopillars. (e) Nanopillars printed on and near micropillars. (f) Higher-magnification view of the 80-nm-diameter nanopillars printed on 2-μm micropillars.

~20 wt %, and the volumetric shrinkage is often more than 60%. It should be noted that microcracks were found on samples having a thickness of more than 2 μm, because of the release of gaseous byproducts during pyrolysis.[38] After pyrolysis, cracks were observed on the films prepared on silicon substrates and carbon cloths, even though the thickness of the films was <500 nm, because of the large differences in expansion coefficients between the precursor and the substrates during heating and cooling. Meanwhile, defect-free ceramics were obtained on the printed freestanding films.

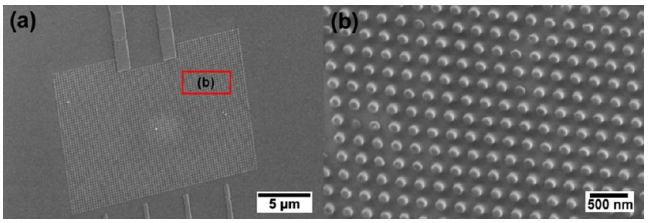

Figure 4. (a) SEM image showing the $SiO_xC_yN_z$ photonic structures after being pyrolyzed at 1100 °C. (b) Higher-magnification micrographs of the ceramic photonic structure indicated in panel (a).

The conversion of preceramic polymers to amorphous ceramic nanostructures was confirmed by different analytical techniques, as shown in Figure 5. Chemical changes during pyrolysis were revealed by FTIR analysis. Significant reduction in intensities of all bands was observed after PUS was cross-linked at 190 °C (Figure 5a). Moreover, the disappearance of the absorption bands of the vinyl group at 3048 and 1592 cm^{-1} indicates that complete cross-linking took place after curing the sample at 190 °C. After pyrolysis, several overlapped bands are observed between 600 cm^{-1} and 1200 cm^{-1}, which can be attributed to the Si−O, Si−C, and Si−N bondings. X-ray photoelectron spectroscopy (XPS) shows the presence of Si, C, N, and O in both samples before and after pyrolysis (see Figure 5b). The binding energies of all elements were found to be ∼0.6 eV lower than those measured before pyrolysis. Results collected from four different samples suggest the existence of Si−C, Si−N, and Si−O networks. The atomic concentration collected from these samples (after pyrolysis) also shows consistent compositions of ∼13% Si, 55.2% C, 5.2% N, and 26.6% O. Since the silazane precursor was prepared and cured in air, a high amount of oxygen contamination in the final ceramics is expected. Both FTIR and XPS results confirm that the composition of the product is $SiO_xC_yN_z$ ceramics. It has been reported that the structure of pyrolytic products are sensitive to the cross-linking processing and pyrolysis conditions. To learn more about the structure of the produced ceramics, we carried out XRD analysis of the cross-linked and pyrolyzed samples. XRD patterns shown in Figure 5c detected a clear reflection at $2\theta = 26.6°$ in the pyrolyzed samples, revealing the presence of graphite in the ceramic products. The Raman spectra shown in Figure 5d reveals the signal of vinyl group at 3050 cm^{-1}, which is an indication of polymerization reactions that caused the liquid precursor to solidify. The visible rising of the C═C band at ∼1500 cm^{-1} in the pyrolyzed PUS confirms the existence of the carbon bonds in the pyrolyzed sample.

Previously, we have shown the influence of viscosity on the efficacy of the printing process, particularly when printing multiple nanofeatures over a landscape of micropatterns.[36] The low-viscosity (0.05−0.2 Pa s) PUS that has been used in this report enables efficient low-pressure filling over a broad range of nanodimensions with a relatively high aspect ratio. The direct molding of high-aspect-ratio ceramic structures has never

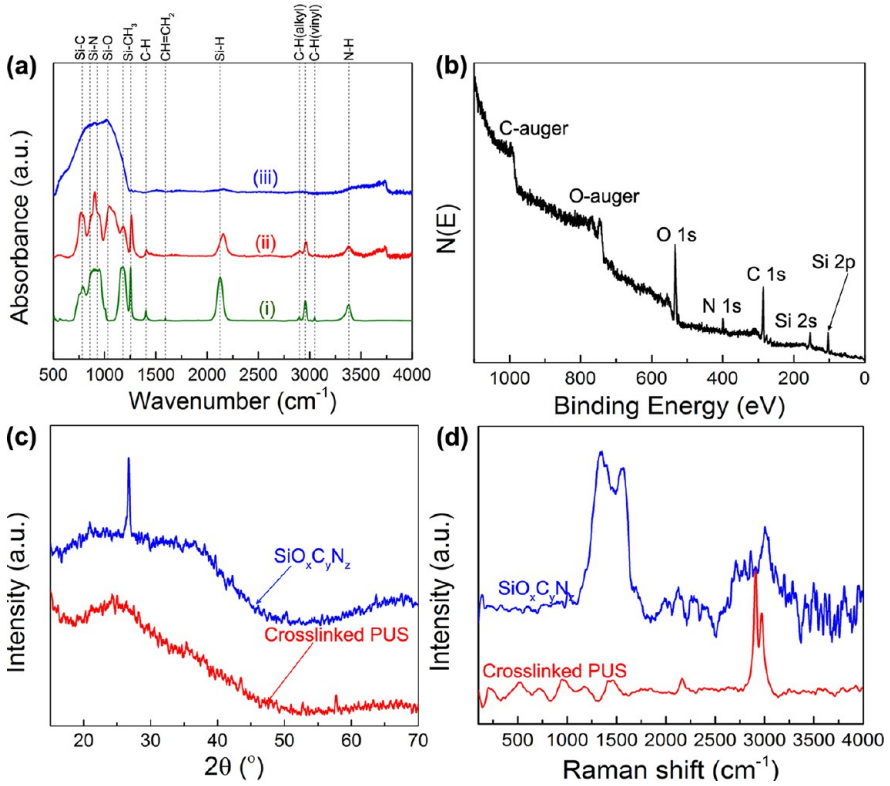

Figure 5. Different characterization techniques were employed to evaluate the samples before and after pyrolysis. (a) FTIR spectra depict significant changes in chemical structures of (i) the starting PUS sample, (ii) cross-linked PUS and $SiO_xC_yN_z$. After pyrolysis, most of the absorption bands disappear except for several overlapped broad bands between 600 cm^{-1} and 1200 cm^{-1}, which attribute to the Si−O, Si−C, and Si−N bondings. (b) The XPS data are in good agreement with FTIR results. XPS analysis suggests the existence of Si−C, Si−O, and Si−N networks in the samples after pyrolysis. Consistent compositions of ∼13% Si, 55.2% C, 5.2% N, and 26.6% O were obtained from four different samples. (c) XRD patterns showing a clear reflection at $2\theta = 26.6°$ in the pyrolyzed samples, revealing the presence of graphite in the ceramic products. (d) Raman analysis shows the evolution of characteristic carbon (C═C) structures in the pyrolyzed sample.

dx.doi.org/10.1021/am400587z | ACS Appl. Mater. Interfaces 2013, 5, 3894−3899

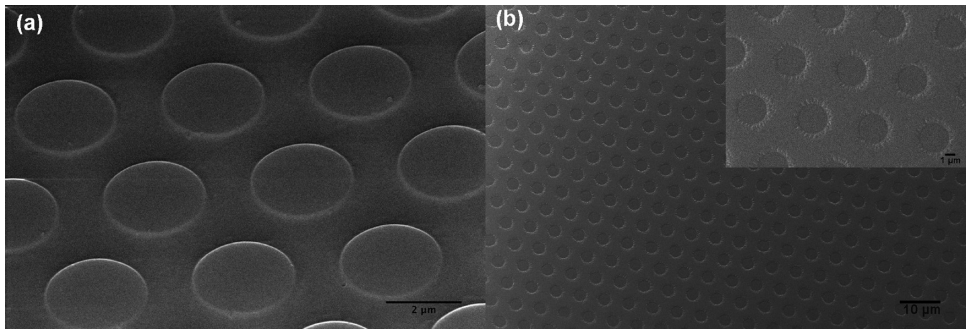

Figure 6. (a) SEM image of the printed PUS microstructures on a silicon substrate. (b) SEM image of microholes printed on the PMMA film using the mold shown in panel (a). The inset in panel (b) shows a higher-magnification image of the microhole arrays.

been demonstrated, to the best of our knowledge, particularly in features ∼100 nm in size. In addition, feature sizes in ceramics are ideally free from any fundamental size limitation, such as in polymers, due to the relatively large molecular size of polymer resists. Metallic glasses and ceramics have the potential to be able to replicate atomic-level features. However, structure replication and printing within the size range from atomic to ∼100 nm is generally dominated by strong capillary forces and wettability of the printing medium on the mold. The strong capillary forces and poor wettability can result in high molding pressure preventing faithful replication of high-aspect-ratio ceramic structures, particularly when the size range approaches 100 nm or smaller. Modified Hagen-Poisseuille's relationship developed in ref 36 combines viscous and capillary contributions at elevated temperatures for polymers for an accurate description of printing pressure on nanometer length scales. However, for such a low-viscosity medium, the printing pressure is predominantly determined by the contact angle and printing length scales, both of which are intimately related and can be described as $P = (4\gamma/d)\cos\theta \times (\chi - 1)$, where $\chi = (8m^2\gamma\eta_T/t\cos\theta) \times d$, which is $\ll 1$. Here, η_T is the viscosity at temperature T, γ the ceramic precursor−vacuum interfacial energy (∼1 N m^{-1}), θ the dynamic contact angle between the printing medium and nanostructure mold, t the filling time (∼1 s), m the aspect ratio, and d the diameter of the nanoasperities to be filled. Within the wetting regime ($\theta < \pi/2$), for a viscosity of 0.2 Pa s, one can safely assume that P (Pa) $\approx -(\cos\theta/D)$, which offers a negative imprinting pressure and indicates spontaneous self-filling of the nanoasperities.

The key advantage of using a ceramic precursor as the printing medium is that the printed structure can be transferred to ceramics with essentially the same dimensions but an inverted structure. The conversion of the precursor to ceramic will allow the fabrication of a second-generation mold with essentially the same material but with different wetting properties. This allows the imprinting process to be further extended to the nanometer scale with printing media otherwise not printable because of poor wetting properties on silicon molds. Modification of the contact angle with different nanostructures is well-established in the literature,[39] and it can be derived from energy arguments as $\cos\theta = (1 - \varphi_s)(r - \varphi_s)$, where φ_s is the nonwetted solid fraction ($\varphi_s = (\pi d^2/4p^2)$) and r is the ratio of the real surface area to the horizontal projection of the surface area ($r = 1 + (\pi dh/p^2)$, with h being the height (or depth) of the nanoasperities and p being the center-to-center pitch). Figure 3 shows printed preceramic structures with different dimensions offering a unique possibility of tuning contact angles for second- and third-generation printed molds.

A current challenge facing NIL is the ability to completely remove polymers from the mold surface after each printing, which can be achieved either by applying a releasing agent or lowering the surface adhesion of the mold. We found that the second-generation pattern can easily be removed from the PUS mold without any surface modification, even after more than 10 consecutive printings. Figure 6a shows the top view of the PUS printed micropillars. This replica served as a mold to print the poly(methyl methacrylate) (PMMA) microholes, using a nanoimprint by melt processing (NIMP) technique,[36] as shown in Figure 6b. To investigate the releasing behavior of the printed PUS mold, we measured contact angles of a silicon substrate in comparison to printed PUS structures before and after converting them to ceramic. Our results show that the contact angle of water on a silicon substrate is 47°, while it is 98° and 77° on printed PUS before and after pyrolysis, respectively. A smaller contact angle for the sample after heat treatment is expected, because of the removal (burning) of the organic side chains and functional groups present in PUS. Note that the contact angle reported in the manuscript is measured on a flat sample and is expected to decrease further, once nanostructured.[36] The contact angle of the cured preceramic polymer is comparable to the reported value of poly(dimethylsiloxane) (PDMS, 90°−120°).[40] The softness of an elastomer such as PDMS limits the aspect ratio of relief features in soft lithography between 0.2 and 2.[41] This drawback can be substantially improved by using a preceramic polymer, because an ultrahigh aspect ratio of ∼20:1 microsized preceramic structures can be achieved.[42] In addition, cured PDMS can be swelled in many nonpolar organic solvents,[43] while cured PUS is highly resistant to numerous solvents, water, and even dilute acids and bases.[23] Furthermore, the cured preceramic polymer is optically transparent down to 300 nm;[23] hence, it is suitable for printing/molding UV-curable polymers. These results indicated that the PUS mold is a potential candidate as a mold material for NIL as well as soft lithography applications, because it simultaneously solves many current technical problems that exist in both techniques.

4. CONCLUSION

In summary, we have proposed a new printing method called spin-on nanoprinting (SNAP) lithography and demonstrated its feasibility of fabricating sub-100 nm ceramic patterns. Moreover, no damage was observed on the silicon master mold, even after more than 20 repetitive printing. Reproduction of fine structures on a large-area printing (5 cm × 5 cm) is also

viable by SNAP lithography within <5 min, which also set a processing time benchmark against other conventional and unconventional lithography. The printed preceramic structures can serve as the molds for printing second-generation patterns of various polymeric materials. We believe the simplicity, versatility, short processing time, and high-fidelity replica make our technique highly favorable for developing nanodevices.

AUTHOR INFORMATION

Corresponding Author

*E-mail: Jayan.Thomas@ucf.edu.

Author Contributions

The manuscript was written through contributions of all authors. All authors have given approval to the final version of the manuscript. J.T. was responsible for administering the project, project planning, and project execution.

Notes

The authors declare no competing financial interest.

ACKNOWLEDGMENTS

The authors thank Materials Characterization Facility (AMPAC), the University of Central Florida and University Spectroscopy & Imaging Facility (USIF), University of Arizona for the sample characterization. We also acknowledge University of California, Santa Barbara (UCSB) for mold fabrication. J.T. acknowledges the University of Central Florida for the financial support.

REFERENCES

(1) Fang, X.; Wu, L.; Hu, L. *Adv. Mater.* **2011**, *23*, 585−598.
(2) Xia, Y. N.; Yang, P. D.; Sun, Y. G.; Wu, Y. Y.; Mayers, B.; Yin, Y. D.; Kim, F.; Yan, H. *Adv. Mater.* **2003**, *15*, 353−389.
(3) Gautam, U. K.; Imura, M.; Rout, C. S.; Bando, Y.; Fang, X. S.; Dierre, B.; Sakharov, L.; Govindaraj, A.; Sekiguchi, T.; Golberg, D.; Rao, C. N. R. *Proc. Natl. Acad. Sci., U.S.A.* **2010**, *107*, 13588−13592.
(4) Lieber, C. M.; Wang, Z. L. *MRS Bull.* **2007**, *32*, 99−104.
(5) Sinitskii, A.; Tour, J. M. *J. Am. Chem. Soc.* **2010**, *132*, 14730−14732.
(6) Sanchez, C.; Belleville, P.; Popall, M.; Nicole, L. *Chem. Soc. Rev.* **2011**, *40*, 696−753.
(7) Tran, H. D.; Li, D.; Kaner, R. B. *Adv. Mater.* **2009**, *21*, 1487−1499.
(8) Parker, A. R.; Townley, H. E. *Nature Nanotechnol.* **2007**, *2*, 347−353.
(9) Sotiropoulou, S.; Sierra-Sastre, Y.; Mark, S. S.; Batt, C. A. *Chem. Mater.* **2008**, *20*, 821−834.
(10) Amsden, J. J.; Domachuk, P.; Gopinath, A.; White, R. D.; Dal Negro, L.; Kaplan, D. L.; Omenetto, F. G. *Adv. Mater.* **2010**, *22*, 1746−1749.
(11) Xia, Y. N.; Whitesides, G. M. *Angew. Chem., Int. Ed.* **1998**, *37*, 551−575.
(12) Black, C. T.; Ruiz, R.; Breyta, G.; Cheng, J. Y.; Colburn, M. E.; Guarini, K. W.; Kim, H. C.; Zhang, Y. *IBM J. Res. Dev.* **2007**, *51*, 605−633.
(13) Soljacic, M.; Joannopoulos, J. D. *Nat. Mater.* **2004**, *3*, 211−219.
(14) Liu, Y.; Liew, L.; Luo, R.; Cross, T.; An, L.; Dunn, M. L.; Daily, J. W.; Raj, R. *Sens. Actuators A* **2002**, *95*, 143−151.
(15) Maksimovic, M.; Stojanovic, G. M.; Radovanovic, M.; Malesev, M.; Radonjanin, V.; Radosavljevic, G.; Smetana, W. *Constr. Build. Mater.* **2012**, *26*, 327−333.
(16) Wu, C. H.; Zorman, C. A.; Mehregany, M. *Thin Solid Films* **1999**, *355*, 179−183.
(17) Riedel, R.; Kleebe, H. J.; Schonfelder, H.; Aldinger, F. *Nature* **1995**, *374*, 526−528.
(18) Kang, W.; Saif, M. T. A. *J. Micromech. Microeng.* **2011**, *21*, 105017.1−105017.11.
(19) Fang, F.; Liu, K.; Kurfess, T.; Lim, G., Tool-based micro-machining and applications in MEMS/NEMS. In *Handbook Techniques and Applications*, Leondes, C. T., Ed.; Springer: New York, 2006; Vol. *1*, pp 678−740.
(20) Colombo, P.; Mera, G.; Riedel, R.; Soraru, G. D. *J. Am. Ceram. Soc.* **2010**, *93*, 1805−1837.
(21) Schulz, M. *Adv. Appl. Ceram.* **2009**, *108*, 454−460.
(22) Vakifahmetoglu, C. *Adv. Appl. Ceram.* **2011**, *110*, 188−204.
(23) Kion VL20 and Ceraset SN liquid polysilazanes technical notes. http://www.kiondefense.com/bulletins/TB1.pdf (accessed Jan. 7, 2011).
(24) Fukuyama, S.; Shin, D.; Komatsu, Y.; Harada, H.; Nakata, Y.; Kobayashi, M.; Okura, Y. *Process for forming silicon dioxide film.* U.S. Patent 5,770,260, Nov. 2, 1999.
(25) Seisyan, R. P. *Tech. Phys.* **2011**, *56*, 1061−1073.
(26) Zhao, X. M.; Xia, Y. N.; Whitesides, G. M. *Adv. Mater.* **1996**, *8*, 837−840.
(27) Kim, E.; Xia, Y. N.; Zhao, X. M.; Whitesides, G. M. *Adv. Mater.* **1997**, *9*, 651−654.
(28) Schulz, M.; Borner, M.; Gottert, J.; Hanemann, T.; Hausselt, J.; Motz, G. *Adv. Eng. Mater.* **2004**, *6*, 676−680.
(29) Chou, S. Y.; Krauss, P. R.; Renstrom, P. J. *Appl. Phys. Lett.* **1995**, *67*, 3114−3116.
(30) Guo, L. J. *Adv. Mater.* **2007**, *19*, 495−513.
(31) Guo, L. J. *J. Phys. D Appl. Phys.* **2004**, *37*, R123−R141.
(32) Jang, Y. S.; Jank, M.; Maier, V.; Durst, K.; Travitzky, N.; Zollfrank, C. *J. Eur. Ceram. Soc.* **2010**, *30*, 2773−2779.
(33) Park, S.; Park, H. H.; Han, O. H.; Chae, S. A.; Lee, D.; Kim, D. P. *J. Mater. Chem.* **2010**, *20*, 9962−9967.
(34) Turcotte, D. E.; Lockwood, F. E.; Baumgart, R. J.; Dituro, M. A.; Phoenix, C. S. *Water Repellent Glass Treatment For Automotive Applications.* U.S. Patent 6,461,537, Oct. 8, 2002.
(35) Pierce, S. M.; Chan, K. B.; Zhu, H. P. *J. Agric. Food Chem.* **2008**, *56*, 213−219.
(36) Thomas, J.; Gangopadhyay, P.; Araci, E.; Norwood, R. A.; Peyghambarian, N. *Adv. Mater.* **2011**, *23*, 4782−4787.
(37) Leo, A.; Andronenko, S.; Stiharu, I.; Bhat, R. B. *Sensors* **2010**, *10*, 1338−1354.
(38) Janakiraman, N.; Aldinger, F. *J. Eur. Ceram. Soc.* **2009**, *29*, 163−173.
(39) Martines, E.; Seunarine, K.; Morgan, H.; Gadegaard, N.; Wilkinson, C. D. W.; Riehle, M. O. *Nano Lett.* **2005**, *5*, 2097−2103.
(40) Armani, D.; Liu, C.; Aluru, N. Reconfigurable fluid circuits by PDMS elastomer micromachining. *Proceedings of the 12th Micro Electro Mechanical Systems*, Orlando, FL, Jan. 17−21, 1999; pp 222−227.
(41) Delamarche, E.; Schmid, H.; Michel, B.; Biebuyck, H. *Adv. Mater.* **1997**, *9*, 741−746.
(42) Cross, T.; Liew, L.-A.; Bright, V. M.; Dunn, M. L.; Daily, J. W.; Raj, R. Fabrication process for ultra high aspect ratio polysilazane-derived MEMS. *Proceedings of the 15th Annual International Conference on MEMS*, Las Vegas, NV, Jan. 20−24, 2002; pp 172−175.
(43) Lee, J. N.; Park, C.; Whitesides, G. M. *Anal. Chem.* **2003**, *75*, 6544−6554.